



## PEM Fuel Cell Start-up/Shut-down Losses vs Temperature for Non-Graphitized and Graphitized Cathode Carbon Supports

Thomas Mittermeier,<sup>a,\*</sup> Alexandra Weiß,<sup>a,\*</sup> Frédéric Hasché,<sup>a</sup> Gerold Hübner,<sup>b</sup> and Hubert A. Gasteiger<sup>a,\*\*</sup>

<sup>a</sup>Chair of Technical Electrochemistry, Department of Chemistry and Catalysis Research Center, Technical University of Munich, D-85748 Garching, Germany

<sup>b</sup>Volkswagen Aktiengesellschaft, D-38436 Wolfsburg, Germany

One of the key figures for the success of proton exchange membrane fuel cells (PEMFCs) in automotive applications is lifetime. Damage of the cathode carbon support, induced by hydrogen/air fronts moving through the anode during start-up/shut-down (SUSD), is one of the lifetime limiting factors. In this study, we examine the impact of varying the temperature at which SUSD events take place, both experimentally and by a kinetic model. For MEAs with conventional carbon supports, the model prediction of carbon oxidation reaction (COR) currents as a function of temperature matches well with the temperature dependence of experimentally determined SUSD degradation rates (predicting  $\approx 8$ -fold lower COR currents compared to  $\approx 10$ -fold lower measured degradation rates at  $5^\circ\text{C}$  compared to  $80^\circ\text{C}$ ). This, however, is not the case for MEAs with graphitized carbon supports, where a factor of  $\approx 39$  lower COR currents are predicted when decreasing SUSD temperature from  $80$  to  $5^\circ\text{C}$ , in contrast to the measured decrease by a factor of  $\approx 10$ . As we will show, this is explained by a change of the governing degradation mechanism from predominantly carbon corrosion induced losses at higher temperature to predominantly voltage cycling induced platinum surface area losses near/below room temperature.

© The Author(s) 2016. Published by ECS. This is an open access article distributed under the terms of the Creative Commons Attribution Non-Commercial No Derivatives 4.0 License (CC BY-NC-ND, <http://creativecommons.org/licenses/by-nc-nd/4.0/>), which permits non-commercial reuse, distribution, and reproduction in any medium, provided the original work is not changed in any way and is properly cited. For permission for commercial reuse, please email: [oa@electrochem.org](mailto:oa@electrochem.org). [DOI: 10.1149/2.1061702jes] All rights reserved.



Manuscript submitted November 15, 2016; revised manuscript received December 19, 2016. Published December 31, 2016.

With the launch of the *Hyundai Tucson/ix35 Fuel Cell* mid 2014,<sup>1</sup> the *Toyota Mirai* in late 2014,<sup>2</sup> and the *Honda Clarity* in 2016,<sup>3</sup> the first commercial proton exchange membrane fuel cell (PEMFC) electric vehicles were introduced into the automotive market. While this demonstrates a technology readiness level (TRL) as high as TRL 9, thus a proven ability for operation from component to system level,<sup>4</sup> several practical aspects of automotive PEMFC operation remain challenging to date.<sup>5</sup> One such phenomenon is the degradation caused by start-up and/or shut-down (SUSD) of the PEMFC, where a  $\text{H}_2/\text{air}_{\text{anode}}$  gas front moves through the anode flow-field, which was first discussed in the scientific literature by Reiser et al.<sup>6</sup> in 2005 (note that it was described in the patent literature as early as 2002<sup>7</sup>). Typically, during an uncontrolled shut-down, air will leak slowly into the  $\text{H}_2$  compartment through leaks in the back-pressure valve, through the stack sealing or by crossover through the membrane, which was found to lead to substantial damage of the cathode catalyst carbon support in the MEA (membrane electrode assembly).<sup>6</sup> One of the early methods to mitigate this damage was the use of a controlled shut-down, in which a high-flow air purge of the anode compartment was applied in order to minimize the  $\text{H}_2/\text{air}_{\text{anode}}$  front residence time, which is proportional to the induced damage.<sup>8</sup>

The reactions occurring during the passing of the  $\text{H}_2/\text{air}_{\text{anode}}$  front through the anode flow-field are listed in Figure 1a (slightly modified from what was shown in Ref. 9 and 10), illustrating the partially  $\text{H}_2$ -filled (lower left segment, colored in red) and partially air-filled (upper left segment, colored in blue) anode, opposite of the air-filled cathode flow-field (right blue segments) and separated by the proton conducting membrane (orange). While electrons can be well conducted in-plane, mainly via the diffusion media (DM) and flow fields (FF), the in-plane proton conduction resistance through the membrane is very high, so that significant proton conduction in-plane can be supported only over very short distances across the  $\text{H}_2/\text{air}_{\text{anode}}$  front, namely over a distance on the order of ca. 6 times the membrane thickness.<sup>6</sup> Therefore, an SUSD event can be approximated by a fuel cell (lower part of Figure 1b) which is electrically short-circuited with an electrolytic

cell (upper part of Figure 1b). From this it is easy to see that this conceptual fuel cell (FC), represented by the  $\text{H}_2$ -filled part of the anode and by its adjacent cathode, will provide electrical power from the hydrogen oxidation and oxygen reduction reaction (HOR and ORR) shown in the lower part of Figure 1a. The voltage provided by this conceptual fuel cell will drive the electrolysis reactions in the electrolytic part of the cell (EL), namely the ORR on the *anode* and both the oxygen evolution and carbon oxidation reaction (OER and COR) on the *cathode*, as shown in the upper part of Figure 1a. The oxidation of the carbon support on the cathode side leads to a weight loss of carbon, resulting in a thinning of the *cathode* catalyst layer,<sup>6</sup> and, ultimately, in its structural collapse. This is accompanied by a substantial increase in the oxygen transport resistance, so that the SUSD induced voltage losses increase with increasing current density.<sup>11,12</sup>

While the SUSD degradation rate can be reduced by applying a high flow rate air-purge prior to start-up or following a shut-down, i.e., by minimizing the  $\text{H}_2/\text{air}_{\text{anode}}$  front residence time,<sup>8</sup> this would still lead to excessive damage over a very large number of SUSD events (e.g., for car applications, almost 40,000 SUSD cycles would have to be tolerated over vehicle lifetime<sup>13</sup>), so that additional system-related mitigation strategies are required (details can unfortunately only be found in the patent literature),<sup>14</sup> namely partial stack shorting during start-up and shut-down and, most effectively, devising means by which  $\text{H}_2$  can be kept in the anode after shut-down for extended periods of time (hours, even days). Owing to the latter strategy, damaging SUSD events would mostly occur near or below room temperature (e.g., air-intrusion and start-up after very long down-time), so that the quantification of SUSD degradation rates near/below room temperature is quite relevant. However, accelerated SUSD aging tests have predominantly been conducted at/near fuel cell operating temperatures, i.e., at  $65^\circ\text{C}$ ,<sup>6</sup> or  $80^\circ\text{C}$ ,<sup>12</sup> and very few data are available at lower temperatures (to our knowledge, none at/below room temperature). As one would expect, SUSD degradation rates decrease with temperature, as was reported in several patents by General Motors for temperatures ranging from  $30 - 80^\circ\text{C}$ .<sup>8,15</sup> Later on, Lim et al. examined SUSD degradation between  $60^\circ\text{C}$  and  $90^\circ\text{C}$ , but since they maintained a constant water partial pressure, the relative humidity (RH) also varied with temperature, so that temperature and RH effects cannot be deduced independently.<sup>16</sup> Only in the studies by Kreitmeier et al.<sup>17</sup> and by Jo et al.<sup>18</sup> the temperature was varied while

\*Electrochemical Society Student Member.

\*\*Electrochemical Society Fellow.

<sup>†</sup>E-mail: [thomas.mittermeier@tum.de](mailto:thomas.mittermeier@tum.de)

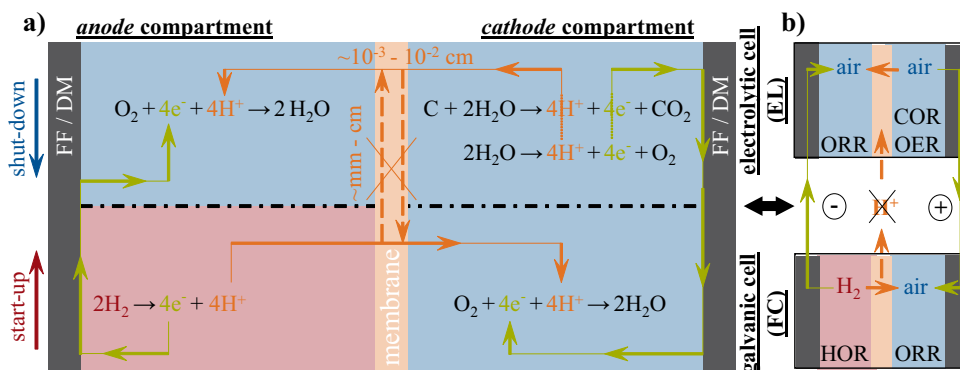


**Figure 1.** Schematic of a start-up and/or shut-down (SUSD) event in a PEMFC, sketching the passage of a  $\text{H}_2/\text{air}_{\text{anode}}$  front through the anode flow-field ( $\text{H}_2$ -filled regions in red, air-filled regions in blue) while the cathode flow-field is filled with air. **a)** Illustration of the reactions occurring during the SUSD event, with sketched pathways of electrons (in green) through the electrode, diffusion medium (DM) and flow-field (FF) as well as of protons (in orange) across the membrane; **b)** Conceptual separation into a fuel cell (FC) segment and an electrolytic cell (EL) segment ( $\text{H}_2$ -filled and air-filled flow-field segments are indicated in red and in blue, respectively). In-plane proton conduction is only possible within very short distances from the  $\text{H}_2/\text{air}_{\text{anode}}$  front ( $\approx 120 \mu\text{m}$  for a  $20 \mu\text{m}$  thick membrane) and not over extended distances, which is indicated by the crossed-out arrows.

keeping RH constant, reporting temperature dependent SUSD degradation over an overall range from  $35\text{--}90^\circ\text{C}$ . These studies were conducted with cathode catalysts based on conventional carbon supports and, to our knowledge, no temperature dependent SUSD degradation rates have been determined with graphitized carbon supports, which exhibit roughly 5-fold lower SUSD degradation rates at  $80^\circ\text{C}$  compared to conventional non-graphitized carbons.<sup>12</sup> In summary, while in current PEMFC systems damaging  $\text{H}_2/\text{air}_{\text{anode}}$  front events are expected to occur only near/below room temperature, no SUSD degradation rate data are available under these conditions, particularly not for graphitized carbon supports, even though these might be useful for developing new and improving existing mitigation strategies.<sup>19–21</sup>

Therefore, we performed  $50 \text{ cm}^2$  single-cell SUSD aging tests covering a wide temperature range from  $5\text{--}80^\circ\text{C}$  with MEAs containing platinum cathode catalysts supported on either conventional or graphitized carbon supports. The MEA performance loss over the SUSD cycling was determined from polarization curves measured at  $80^\circ\text{C}$ . Further, we applied a quasi-steady-state one-dimensional model developed by Gu et al.<sup>22</sup> to predict the temperature dependence of the SUSD degradation rates for the two different types of carbon support. The experimental SUSD degradation rates and the model predictions agree reasonably well and only deviate at low temperatures for the graphitized carbon supports, where voltage cycling induced platinum losses dominate the MEA performance decay rather than carbon corrosion.

## Experimental

**Hardware, set-up and materials.**—PEM fuel cell testing was performed on a customized G60 test station (Greenlight Innovation Corp.). All SUSD experiments were carried out with  $50 \text{ cm}^2$  active area single cells, in either commercial fuel cell hardware (Fuel Cell Technologies, Inc.) or a modified version with additional coolant channels, allowing for water cooling of the endplates. Both configurations utilized quadruple serpentine graphite flow-fields (Fuel Cell Technologies, Inc.) with gases flowing in counter-flow configuration. The MEA, i.e., the catalyst coated membrane (CCM) placed in between two gas diffusion layers (SIGRACET 25BC, SGL Carbon GmbH) was sandwiched between the two flow-field plates. The gas diffusion layer compression of ca. 20% (corresponding to  $\approx 1.5 \text{ MPa}$  compression pressure on the flow-field lands) was assured by choosing the appropriate thickness of nearly incompressible PTFE coated fiberglass subgaskets (Fiberflon GmbH). Two different CCM types with anode/cathode platinum loadings of  $0.1/0.4 \text{ mg}_\text{Pt}/\text{cm}^2$  were tested in this study: i) a commercial CCM (Primea Mesga A510.1/M715.18/C580.4, W. L. Gore GmbH) featuring a platinum cathode catalyst with a

conventional high-surface area carbon support as well as an  $18 \mu\text{m}$  reinforced perfluorsulfonic acid membrane (all CCMs of this type are denominated “conventional C” throughout this work); ii) a CCM with platinum catalysts supported on a graphitized high-surface area carbon support (denominated “graphitized C”), which was fabricated by hot-pressing a sandwich of a catalyst coated anode decal (D-0708, Greenerity GmbH), a  $15 \mu\text{m}$  reinforced low equivalent weight perfluorsulfonic acid membrane (Asahi Kasei Corp.), and a cathode decal (D-0682, Greenerity GmbH) at  $155^\circ\text{C}$  and  $1.5 \text{ MPa}$  for 2 min. Details about materials properties can be found in Table I.

**Gas flow scheme for SUSD experiments.**—Sharp  $\text{H}_2/\text{air}_{\text{anode}}$  shut-down fronts (from  $\text{H}_2$ -filled anode to air<sub>anode</sub>-filled anode) and air<sub>anode</sub>/ $\text{H}_2$  start-up fronts (from air<sub>anode</sub>-filled anode to  $\text{H}_2$ -filled anode) were created by switching between two constantly flowing gas streams on the anode side of the fuel cell,  $\text{H}_2$  and air<sub>anode</sub>, with each gas stream controlled at the same temperature, pressure, and humidity (separate humidifier for  $\text{H}_2$  and air<sub>anode</sub> gas stream). The upper part of Figure 2 illustrates the gas flows and the valve positions for a shut-down/start-up sequence, while the lower part shows a typical resulting voltage profile. During fuel cell operation (segment a), the four shown pneumatic valves are configured such that  $\text{H}_2$  reaches the fuel cell anode, while the air<sub>anode</sub> gas stream is directed to the exhaust via a separate backpressure regulator (not depicted). By switching all four valves simultaneously, both pathways cross over, such that the  $\text{H}_2$  gas stream bypasses the fuel cell through the exhaust, while the air<sub>anode</sub> gas flows through the gas line previously delivering  $\text{H}_2$  to the fuel cell anode (segment b). With the switching time of tens of milliseconds for pneumatic valves, a sharp  $\text{H}_2/\text{air}_{\text{anode}}$  shut-down front on the anode side of the fuel cell is created. The lower part of Figure 2 shows the resulting voltage profile vs. time. Note that to our knowledge, this experimental approach, preserving constant pressure, gas velocity, and relative humidity during flow switching is unique in the literature (generally, the air stream on the anode is not humidified, as this requires an additional humidifier). Switching the valves back to their original position results in an equally sharp air<sub>anode</sub>/ $\text{H}_2$  start-up front (segment c) and an exemplary cell voltage profile vs. time is shown in the lower part of Figure 2. Note that one SUSD cycle in this study refers to the sequence of one shut-down event (from  $\text{H}_2$ -filled anode to air filled anode) and one start-up event (air filled anode to  $\text{H}_2$ -filled anode).

**MEA conditioning and  $\text{H}_2/\text{air}$  polarization curves.**—All MEAs were conditioned before the actual SUSD experiments at  $60^\circ\text{C}$ ,  $50 \text{ kPa}_{\text{gauge, inlet}}$  (pressure controlled at cell inlet) with fully humidified (dew point  $60^\circ\text{C}$ )  $\text{H}_2/\text{air}$  (1400/3300 nccm (referenced to

**Table I.** Specifications of the two different CCM types examined in this study, based on platinum cathode catalysts supported on either conventional high-surface area carbon (referred to as “conventional C”) or on graphitized high-surface area carbon (referred to as “graphitized C”).  $A_{Pt}$  and  $R_{Cont}$  were determined via hydrogen underpotential deposition at room temperature and via four-point probe measurements,<sup>23</sup> respectively. Pt loadings and membrane thickness were obtained from the manufacturers; the carbon support BET areas were obtained from Refs. 22 and 13.

Parameter		Value			Unit
		conventional C / graphitized C			
CCM type:					
$A_{Pt}$ (anode)	Platinum surface area (anode)	50	/	42	m <sup>2</sup> /g
$A_{Pt}$ (cathode)	Platinum surface area (cathode)	50	/	42	m <sup>2</sup> /g
$I_{Pt}$ (anode)	Platinum loading (anode)	0.1	/	0.1	mg/cm <sup>2</sup>
$I_{Pt}$ (cathode)	Platinum loading (cathode)	0.4	/	0.4	mg/cm <sup>2</sup>
$A_C$	Carbon surface area	800	/	160	m <sup>2</sup> /g
$I_C$	Carbon loading (cathode)	0.4	/	0.4	mg/cm <sup>2</sup>
$t_{MEM}$	Membrane thickness	18	/	15	μm
$R_{Cont}$	Cross plane resistance	20	/	20	m Ω · cm <sup>2</sup>

$T_0 = 273.15$  K and  $p_0 = 101.3$  kPa), applying eight subsequent cycles of three potentiostatic steps: i) 0.60 V for 45 min, ii) 0.95 V for 5 min, and iii) 0.85 V for 10 min. Initial polarization curves were taken after MEA conditioning and then after each  $n$  cycles of SUSDs, where  $n$  varied between 10 (at SUSD temperature of 80°C) and 300 (at 5°C for graphitized C MEAs), depending on the level of SUSD degradation. All polarization curves were taken at 80°C, a total reactant inlet pressure of 70 kPa<sub>gauge,inlet</sub>, a relative humidity of  $RH = 0.66$  ( $\equiv 66\%$  RH, but defined as fraction throughout the remainder of this work), and controlled H<sub>2</sub>/air stoichiometries of 1.5/1.8 (note: below 0.2 A/cm<sup>2</sup>, constant flows corresponding to the flows at 0.2 A/cm<sup>2</sup> were applied). Polarization curves were acquired from low to high current densities, averaging the cell voltage over the last 10 s at each current density after a 6 minute hold. Prior to each polarization curve, a potentiostatic recovery step at  $U_{Cell} = 0.60$  V (for 2 minutes, with H<sub>2</sub>/air flows of stoichiometries 1.5/1.8 of H<sub>2</sub>/air) was performed.

**SUSD cycling procedure.**—SUSD cycling at different temperatures (5–80°C) was done at a reactant inlet pressure of 50 kPa<sub>gauge,inlet</sub>. The time between applying start-up and shut-down H<sub>2</sub>/air<sub>anode</sub>-fronts

was kept constant at 120 s. For most experiments, the H<sub>2</sub> and air<sub>anode</sub> flows were maintained at 113 nccm (dry gas flows) and humidified to RH values of  $\geq 1.0$  by adjusting the dewpoint either to the cell temperature (at  $\geq 40^\circ\text{C}$ ) or by setting it to 40°C (at  $< 40^\circ\text{C}$ ). The resulting H<sub>2</sub>/air<sub>anode</sub>-front residence time ( $t_{residence}$ ) for SUSD experiments between 5–80°C thus ranges from 1.3–2.4 s (see Equation 20). Different H<sub>2</sub> and air<sub>anode</sub> flows were only applied when examining the residence time effect on SUSD degradation at 80°C ( $t_{residence} = 0.3 - 2.2$  s) and the applied flows are reported there.

Linearized current density dependent SUSD degradation rates (in units of mV/cycle) were obtained from the polarization curves (see above) by determining the number of SUSD cycles required to induce a 50 mV performance loss at any given current density (see Results and Discussion). Since these are essentially independent of  $t_{residence}$  within the examined range (see Results and Discussion), time-normalized linearized SUSD degradation rates (in units of mV/cycle/s) are used to compare the temperature dependence of the measured SUSD degradation.

**Quantification of electrode thicknesses.**—Electrode thicknesses were determined on cut-outs of either pristine CCMs or of DM/CCM/DM sandwiches harvested after SUSD experiments. Five quadratic cut-outs ( $\approx 1 \times 1$  cm<sup>2</sup>) were taken from each sample (one from the center and one from each corner), embedded into a polymer resin, and then ground and polished to a mirror finish. Catalyst layer thicknesses were determined using a benchtop scanning electron microscope (SEM; JCM-6000, JEOL GmbH) which was operated in backscattering mode at an acceleration voltage of 15 kV and a magnification of  $\times 1,000$ . Each cut-out was evaluated at five positions (i.e., 25 measurements per sample) to obtain an average thickness and its standard deviation (represented by error bars).

### Kinetic H<sub>2</sub>/Air<sub>anode</sub> SUSD Model

A one-dimensional quasi-steady-state fuel cell model was employed to predict the temperature dependence of anode H<sub>2</sub>/air<sub>anode</sub> front (SUSD) induced performance degradation by projecting carbon oxidation reaction (COR) currents versus temperature for the two different cathode catalyst supports. The underlying assumptions are that the SUSD degradation rate is directly proportional to the carbon oxidation current ( $i_{COR}$ ) on the fuel cell cathode induced by H<sub>2</sub>/air<sub>anode</sub> fronts as well as that the cathode carbon support oxidation is the only contribution to the measured performance degradation (as shown later, this is true in most cases). The applied model is a slightly modified version of the model presented by Gu et al.,<sup>22</sup> principally considering two conceptually separate but electrically short-circuited electrochemical devices, viz., a fuel cell (FC) and an electrolytic cell (EL) (see Figure 1b). Those are distinguished by the relative position  $\tau$  of the H<sub>2</sub>/air<sub>anode</sub> front moving through the fuel cell ( $\tau \equiv 0$  when the entire anode is filled with air<sub>anode</sub>;  $\tau \equiv 1$  when the entire anode is under H<sub>2</sub>, cf. Figure 1a). Since both devices form a closed electrical circuit, both cell voltage and interchanged total current must

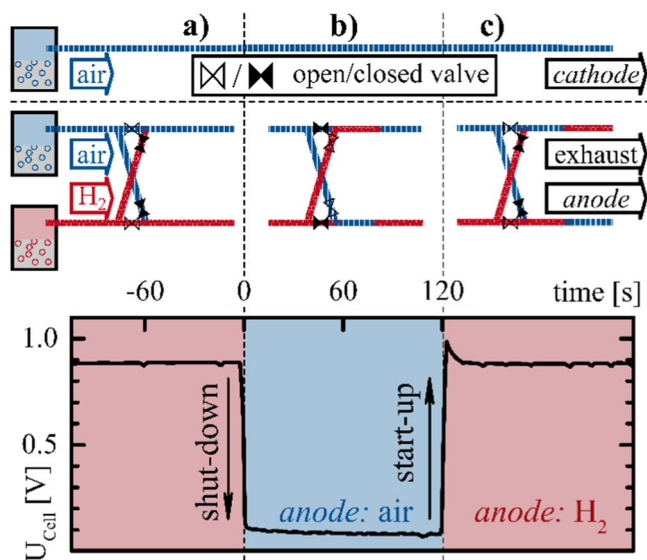


**Figure 2.** The upper part shows the flow switching scheme to generate H<sub>2</sub>/air<sub>anode</sub> fronts for SUSD experiments: a) configuration for normal fuel cell operation; b) application of an H<sub>2</sub>/air<sub>anode</sub> front representing a shut-down process, created by simultaneous switching of the four pneumatic valves; and, c) application of an air<sub>anode</sub>/H<sub>2</sub> front representing start-up, created by repeated switching of the valves. The lower part shows a typical resulting cell voltage profile during switching H<sub>2</sub> and air<sub>anode</sub> on the anode side of a fuel cell while the cathode side is continually fed with air (red segments mark a H<sub>2</sub>-filled anode, blue segments an air-filled anode).

match. In consequence, the quasi-steady-state condition is defined by  $U_{FC} = U_{EL}$ , at which point the same current density ( $i$ ) is flowing through each of the four segments shown in Figure 1a. Even though the model has already been discussed in detail by Gu et al. in Reference 22 we will reproduce parts of it here in order to specify all our model parameters and to indicate the minor differences in the model.

Equation 1 shows the calculation of the cell voltage for the fuel cell part ( $U_{FC}$ )

$$U_{FC} = E_{ORR}^{cathode} - E_{HOR}^{anode} - \eta_{mem}^{FC} - \eta_{cont}^{FC} - \eta_{H^+}^{FC} \quad [1]$$

where  $E_{ORR}^{cathode}$  and  $E_{HOR}^{anode}$  represent the electrode potentials of *cathode* and *anode* in the  $H_2$ -filled segment of the cell (lower part in Figure 1a). The  $\eta$ -terms refer to the overpotentials/voltage losses induced by membrane protonic resistance ( $\eta_{mem}$ ), electrical cross-plane/contact resistances ( $\eta_{cont}$ ), and effective proton conduction resistance in the electrode in which the ORR occurs ( $\eta_{H^+}$ ). An analogous equation can be written for the cell potential ( $U_{EL}$ ) of the conceptual electrolyzer, based on the relevant reactions which are shown in the upper segment of Figure 1a:

$$U_{EL} = E_{OER/COR}^{cathode} - E_{ORR}^{anode} + \eta_{mem}^{EL} + \eta_{cont}^{EL} + \eta_{H^+}^{EL} \quad [2]$$

Here,  $E_{OER/COR}^{cathode}$  is the electrode potential at the *cathode*, where both the oxygen evolution and the carbon oxidation reaction (OER and COR) occur simultaneously (see upper right segment of Figure 1a), and ( $\eta_{H^+}$ ) is the loss by proton conduction resistance in the electrode where OER/COR occurs (we neglect the proton conduction losses in the *anode*, as it has only  $\approx 1/4$  of the thickness of the *cathode*); note that throughout this manuscript we use a static definition of *anode* ( $\equiv$  electrode which is the  $H_2$ -anode under normal operation) and *cathode* ( $\equiv$  electrode which is the air-cathode under normal operation), independent of the actual reactions at the electrodes.  $E_{ORR}^{anode}$  then denotes the electrode potential of the *anode* electrode of the cell, where the oxygen reduction reaction (ORR) occurs in the electrolytic part of the cell (see upper left segment of Figure 1a). Note that capacitive effects are neglected in this model, as the residence times used in our SUSD temperature-dependence study (1.3 – 2.4 s) are long enough for the contributions from capacitive effects to carbon corrosion to be minor and can thus be neglected.<sup>13,22</sup>

For the fuel cell part, the positive electrode (see lower part in Figure 1a) is associated with the oxygen reduction reaction (ORR), and the corresponding electrode potential can be described by Tafel kinetics:

$$E_{ORR}^{cathode} = E_{ORR/OER}^{rev} - \frac{R \cdot T}{\alpha_C \cdot F} \cdot \ln \left[ \frac{i_{ORR}^{cathode}}{i_0 \cdot A_{Pt}^{cathode} \cdot i_{Pt}^{cathode}} \right] \quad [3]$$

Here,  $E_{ORR/OER}^{rev}$  is the reversible potential of the ORR/OER at the given temperature  $T$  and at the applied oxygen partial pressure,  $R$  is the universal gas constant ( $8.314 \text{ J mol}^{-1} \text{ K}^{-1}$ ),  $\alpha_C$  is the cathodic transfer coefficient for the ORR,  $F$  is the Faraday constant ( $96,485 \text{ C mol}^{-1}$ ),  $i_0$  is the exchange current density at the given conditions, and  $A_{Pt}^{cathode}$  and  $i_{Pt}^{cathode}$  are the electrochemically active Pt surface area and the Pt loading of the *cathode* electrode. The electrode potential of the negative electrode of the fuel cell part (see lower part of Figure 1a) is determined by the hydrogen oxidation reaction (HOR) kinetics:

$$E_{HOR}^{anode} = E_{HOR}^{rev} + \frac{R \cdot T}{2 \cdot F} \cdot \frac{i_{HOR}^{anode}}{i_0 \cdot A_{Pt}^{anode} \cdot i_{Pt}^{anode}} \quad [4]$$

where  $E_{HOR}^{rev}$  is the reversible potential of the HOR (note that owing to the fast HOR kinetics on Pt, a Butler-Volmer equation linearized near zero overpotential is used – the highest value in this work is  $\approx 1 \text{ mV}$ ; here the sum of the anodic and cathodic transfer coefficient was assumed to be 2, in accordance with Gu's original model<sup>22</sup>) and the other parameters have the above defined meaning.

For the conceptual electrolytic part of the cell (see upper part of Figure 1a), the *anode* is governed by the ORR, already described by Equation 3 (see upper left part of Figure 1a), while in the *cathode* both the oxygen evolution reaction (OER) and the carbon oxidation reaction (COR) take place (see upper right part of Figure 1a). Hence,

at the *cathode* electrode potential of the electrolytic part of the cell ( $E_{OER/COR}^{cathode}$ ), both OER and COR currents are driven at rates commensurate with this potential:

$$E_{OER/COR}^{cathode} = E_{OER}^{cathode} = E_{COR}^{cathode} \quad [5]$$

Here,  $E_{OER}^{cathode}$  and  $E_{COR}^{cathode}$  are the electrode potentials at which the OER and COR take place, whereby the respective current densities are described by the following Tafel kinetics:

$$E_{OER}^{cathode} = E_{ORR/OER}^{rev} + \frac{R \cdot T}{\alpha_A \cdot F} \cdot \ln \left[ \frac{i_{OER}^{cathode}}{i_0 \cdot A_{Pt} \cdot i_{Pt}^{cathode}} \right] \quad [6]$$

$$E_{COR}^{cathode} = E_{COR}^{rev} + \frac{R \cdot T}{\alpha_A \cdot F} \cdot \ln \left[ \frac{i_{COR}^{cathode}}{i_0 \cdot A_C \cdot i_C^{cathode} \cdot (1 - \Theta)^m} \right] \quad [7]$$

In the latter equation,  $\Theta$  describes the fraction of the carbon-support that has already been oxidized to  $CO_2$ ;  $m$  describes the COR rate dependence on  $\Theta$ , whereby  $m \approx 0$  for graphitized carbons (i.e., the COR is independent of the extent of already oxidized carbon), while  $m$  is a positive number for conventional carbons (e.g.,  $m = 10.4$  for Vulcan<sup>22</sup>), for which the COR decreases as the fraction of oxidized carbon increases.<sup>12,13,22,24</sup> Thus, since  $\Theta$  increases with the number of SUSD cycles, the COR currents for conventional carbon will also decrease. Projecting that the end-of-life carbon loss ( $\Theta_{max}$ ) at an SUSD temperature of  $80^\circ\text{C}$  is likely in the region of 10 wt% ( $\Theta \approx 9 - 10 \text{ wt}\%$  at an SUSD induced voltage loss of 50–100 mV for high-surface area non-graphitized carbon based on Figure 6 in Reference 13), one can calculate an effective average COR current factor for conventional carbon by averaging the  $(1 - \Theta)^m$  term in Equation 7 between  $\Theta = 0$  and  $\Theta = \Theta_{max}$  (i.e.,  $\Theta_{max}^{-1} \cdot \int_0^{\Theta_{max}} d\Theta (1 - \Theta)^m$ ). This yields a value of 0.61 for  $m = 10.4$  and  $\Theta_{max} = 10 \text{ wt}\%$ , which we used to calculate average carbon corrosion currents on conventional carbon electrodes (i.e., the  $(1 - \Theta)^m$  term in Equation 7 was replaced by 0.61 for conventional C MEAs).

At quasi-steady state, the *total* current that is supplied by the fuel cell (lower part in Figure 1b) equals the total current consumed by the electrolytic cell (upper part in Figure 1b) and will be referred to as  $I_{SUSD}$ . The local current *densities* in either part of the cell,  $i_{FC}$  and  $i_{EL}$ , then scale inversely with the relative position of the  $H_2$ /air<sub>anode</sub> front  $\tau$ . In the case of the electrolytic part of the cell, the current density  $i_{EL}$  is thus described by:

$$i_{EL} = \frac{I_{SUSD}}{A_{cell} \cdot (1 - \tau)} = \frac{I_{SUSD}/A_{cell}}{(1 - \tau)} \quad [8]$$

where  $A_{cell}$  refers to the total active area of the entire cell (50  $\text{cm}^2$  in this study). Since in some cases the predicted  $I_{SUSD}$  values are relatively small, the current density in the fuel cell part ( $i_{FC}$ ) was also corrected for the hydrogen crossover current density ( $i_{H_2-cross}$ ).

$$i_{FC} = \frac{I_{SUSD} + A_{cell} \cdot \tau \cdot i_{H_2-cross}}{A_{cell} \cdot \tau} = \frac{I_{SUSD}/A_{cell}}{\tau} + i_{H_2-cross} \quad [9]$$

The value of  $i_{H_2-cross}$  was determined experimentally for each examined SUSD condition (i.e., at various temperatures,  $RH = 1$ , and a total cell pressure of 50  $\text{kPa}_{\text{gauge, inlet}}$ ) and fitted to an Arrhenius type relation, so that it is valid at constant total pressure of 50  $\text{kPa}_{\text{gauge}}$  and  $RH = 1$ :

$$i_{H_2-cross} = \frac{i_{H_2-cross}^*}{t_{mem}} \cdot \left( \frac{p_{H_2}}{p_{H_2}^*} \right) \cdot \exp \left[ - \frac{E_{H_2-cross}^{act}}{R \cdot T} \left( 1 - \frac{T}{353.15} \right) \right] \quad [10]$$

Here,  $i_{H_2-cross}^*$  is the membrane thickness normalized reference hydrogen crossover current at  $80^\circ\text{C}$  and  $p_{H_2}^* = 101.3 \text{ kPa}$ ,  $t_{mem}$  is the membrane thickness,  $E_{H_2-cross}^{act}$  is the associated apparent activation energy, and  $T$  is the temperature in units of Kelvin.

During the SUSD event, the quasi-steady-state current density in the fuel cell part ( $i_{FC}$ ) caused by the flowing SUSD current ( $I_{SUSD}$ ) and described by Equation 9 must equal the HOR current density in the *anode* of the fuel cell part ( $i_{HOR}^{anode}$ ; see Equation 4), which in turn

must equal the ORR current density in the *cathode* of the fuel cell part ( $i_{\text{ORR}}^{\text{cathode}}$ , see Equation 3):

$$i_{\text{FC}} = \frac{I_{\text{SUSD}}/A_{\text{cell}}}{\tau} + i_{\text{H}_2\text{-cross}} = i_{\text{HOR}}^{\text{anode}} = i_{\text{ORR}}^{\text{cathode}} \quad [11]$$

Similarly, quasi-steady-state current density in the electrolytic part ( $i_{\text{EL}}$ ) described by Equation 8 must be matched by the sum of the current densities for the OER and the COR in the *cathode* of the electrolytic part of the cell ( $i_{\text{OER}}^{\text{cathode}}$  and  $i_{\text{COR}}^{\text{cathode}}$  described by Equation 6 and Equation 7, respectively), which in turn must equal the ORR current density in the *anode* ( $i_{\text{ORR}}^{\text{anode}}$ ) of the electrolytic part:

$$i_{\text{EL}} = \frac{I_{\text{SUSD}}/A_{\text{cell}}}{(1-\tau)} = i_{\text{OER}}^{\text{cathode}} + i_{\text{COR}}^{\text{cathode}} = i_{\text{ORR}}^{\text{anode}} \quad [12]$$

Here,  $i_{\text{ORR}}^{\text{anode}}$  is obtained from a Tafel kinetics equation analogous to that given in Equation 3:

$$E_{\text{ORR}}^{\text{cathode}} = E_{\text{ORR/OER}}^{\text{rev}} - \frac{R \cdot T}{\alpha_{\text{C}} \cdot F} \cdot \ln \left[ \frac{i_{\text{ORR}}^{\text{anode}}}{i_0 \cdot A_{\text{Pt}}^{\text{anode}} \cdot i_{\text{Pt}}^{\text{anode}}} \right] \quad [13]$$

The reversible potentials of for all of the above described reactions are obtained from the Nernst equation:

$$E_j^{\text{rev}} = E_j^0 + \Delta E_j \cdot (T - 298.15) + \frac{R \cdot T}{n \cdot F} \cdot \ln \left[ \frac{\prod_k (a_o)_k^{v_o}}{\prod_l (a_r)_l^{v_r}} \right] \quad [14]$$

where  $n$  is the number of electrons,  $T$  is the temperature in Kelvin, and  $a_o/a_r$  are activities of oxidized/reduced species at stoichiometry  $v_o/v_r$ , respectively, defined as the respective gas partial pressures (in kPa) divided by the standard pressure of 101.3 kPa (i.e.,  $a_o = \frac{p_o}{101.3}$  and  $a_r = \frac{p_r}{101.3}$ ); the activity for  $\text{H}_2\text{O}$  was set to 1 as  $\text{RH} = 1$ . The terms  $E_j^0$  and  $\Delta E_j$  represent the standard electrode potentials and its temperature coefficient, respectively, for each of the considered reactions. Nernstian corrections were carried out for  $\text{O}_2$ ,  $\text{H}_2$  and  $\text{CO}_2$ , based on the nominal gas composition (assumed 400 ppm of  $\text{CO}_2$  in air).

The exchange current densities under the actual reactant concentrations ( $i_0$ ) were obtained from the exchange current densities at reference conditions of  $80^\circ\text{C}$  and activities of  $a_j = 1$  ( $i_{00} = i_0|_{T=353.15 \text{ K}, a_j=1}$ ) for the HOR, the ORR, and the OER:

$$i_0 = i_{00} \cdot (a_i)^{\gamma_i} \cdot \exp \left[ -\frac{E_j^{\text{act}}}{R \cdot T} \cdot \left( 1 - \frac{T}{353.15} \right) \right] \quad [15]$$

Here,  $\gamma_i$  is the reaction order with respect to the reactant  $i$ , and  $E_j^{\text{act}}$  is the activation energy for reaction  $j$ . All thermodynamic and kinetic parameters as well as the temperature dependence of the hydrogen crossover current density are given in Table II. For the COR,  $a_{\text{H}_2\text{O}} = 1$  in any case (as was kept  $\text{RH} \geq 1$  during the SUSD cycles), thus the only correction of  $i_{00}$  was carried out via the Arrhenius term in Equation 15.

Having described the kinetic overpotential losses to determine the anode and cathode electrode voltages in Equations 1 and 2, we now describe the equations used to determine the ohmic voltage losses. The voltage loss by proton conduction resistance through the membrane is given by (taken from Ref. 22):

$$\eta_{\text{mem}}^{\text{FC/EL}} = \frac{i_{\text{FC/EL}} \cdot t_{\text{mem}}}{\left( 8.81 \cdot 10^{-2} \cdot \text{RH}^{1.84} \cdot \exp \left[ -\frac{E_{\text{H}^+}^{\text{act}}}{R \cdot T} \cdot \left( 1 - \frac{T}{353.15} \right) \right] \right)} \quad [16]$$

Whereby the  $t_{\text{mem}}$  refers to the membrane thickness (15 or 18  $\mu\text{m}$ ) and the apparent activation energy for proton conduction ( $E_{\text{H}^+}^{\text{act}}$ ) was taken as 6 kJ/mol.<sup>22</sup> The electrical bulk and contact resistances ( $\eta_{\text{cont.}}^{\text{FC/EL}}$ ) were obtained from the measured electronic resistance ( $R_{\text{cont.}} = 20 \text{ m} \Omega \cdot \text{cm}^2$ ) at the given cell compression:

$$\eta_{\text{cont.}}^{\text{FC/EL}} = i_{\text{FC/EL}} \cdot R_{\text{cont.}} \quad [17]$$

Finally, the proton conduction through the *cathode* electrode was determined by the following equation given in Reference 22 and as-

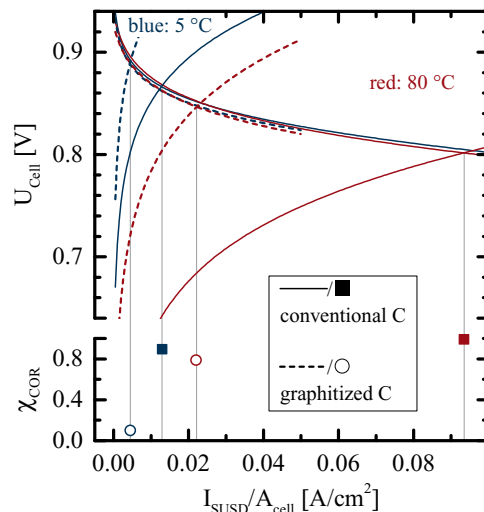


**Figure 3.** Upper part: Modeled polarization curves for both the fuel cell and the electrolytic part of the cell during a SUSD event, plotting  $U_{\text{cell}}$  versus the SUSD current normalized by the entire cell area (i.e.,  $I_{\text{SUSD}}/A_{\text{cell}}$ ) for MEAs with conventional/graphitized carbon supports of the cathode catalysts (full/dashed lines) for 5 and  $80^\circ\text{C}$  (blue and red lines, respectively). The vertical drop lines mark the intersections of the polarization curves for the fuel cell and the electrolytic part of the cell. Lower part: Full/open symbols indicate the fraction of the total current going into the COR (see Equation 19) for MEAs with conventional/graphitized carbon supports. This plot is based on a  $\text{H}_2/\text{air}_{\text{anode}}$  location  $\tau = 0.5$  and a total gas pressure of  $p = 50 \text{ kPa}_{\text{gauge}}$ , at  $\text{RH} \geq 1$ .

suming  $t_{\text{cathode}} = 30 \mu\text{m}/(\text{mg}_{\text{Pt}} \cdot \text{cm}^{-2})$ :

$$\eta_{\text{H}^+}^{\text{FC/EL}} = \frac{i_{\text{FC/EL}} \cdot i_{\text{Pt}}^{\text{cathode}} \cdot t_{\text{cathode}}}{3 \cdot \left( 2.23 \cdot 10^{-2} \cdot \text{RH}^{2.84} \cdot \exp \left[ -\frac{E_{\text{H}^+}^{\text{act}}}{R \cdot T} \cdot \left( 1 - \frac{T}{353.15} \right) \right] \right)} \quad [18]$$

Under the simplifying assumption that the OER in the electrolytic part of the cell can be neglected, an analytical expression for the polarization curve of the electrolytic cell could be obtained. However, in the case of using a cathode catalyst with a graphitized carbon support, the effective potential in the *cathode* of the electrolytic part of the cell increases to values at which the OER currents become substantial, so that this simplifying assumption is not anymore satisfied.<sup>22</sup> Therefore, the value of the SUSD current ( $I_{\text{SUSD}}$ ) was determined by first evaluating the cell voltage versus the effective current density ( $I_{\text{SUSD}}/A_{\text{cell}}$ ) for the fuel cell part of the cell (HOR on the *anode* and ORR on the *cathode*) and for the electrolytic part of the cell (ORR on the *anode* and COR/OER on the *cathode*), in which case the quasi-steady-state  $I_{\text{SUSD}}/A_{\text{cell}}$  value could be obtained from the intersection of the two polarization curves. This is shown in Figure 3 for a  $\text{H}_2/\text{air}_{\text{anode}}$  front position of  $\tau = 0.5 \text{ s}$ , which is generally considered to be a good estimate for obtaining the  $\tau$ -averaged SUSD current (discussed in Reference 22 and verified later on). For both conventional C MEAs (solid lines in Figure 3) and graphitized C MEAs (dashed lines in Figure 3), the cell voltage curve for the fuel cell part of the cell (monotonically decreasing lines) are, as one would expect, essentially identical. There is also very little difference with temperature of the fuel cell polarization curves at  $80^\circ\text{C}$  (red lines) compared to  $5^\circ\text{C}$  (blue lines), which is due to the very low activation energy if evaluated at constant cell potential, as described by Neyerlin et al.<sup>26</sup> On the contrary, the polarization curves for the electrolytic part of the cell (monotonically increasing lines in Figure 3) show a very strong dependence on both temperature and carbon type, which is due to the very high activation energy for the COR (see Table II). The quasi-steady-state SUSD current density (expressed as  $I_{\text{SUSD}}/A_{\text{cell}}$  shown as x-axis in Figure 3) flowing through both the fuel cell and the electrolytic part of the cell corresponds to the intersection of the respective fuel cell and electrolytic cell

**Table II. Kinetic parameters used in the SUSD model (the references from which the parameters were obtained are given in parentheses for each reaction). Hydrogen crossover was determined experimentally as a function of temperature at constant total pressure of 50 kPa<sub>gauge</sub> and fitted to Equation 10 for RH ≥ 1.0 experimentally.**

Parameter		Value	Unit
<i>HOR</i> <sup>21,24</sup>			
$i_{00}$	Exchange current density at reference conditions (80°C, 101.3 kPa H <sub>2</sub> )	0.3	A/cm <sup>2</sup> <sub>Pt</sub>
$E^{\text{act}}$	Activation energy	10	kJ/mol
$\gamma$ (H <sub>2</sub> )	Hydrogen reaction order	1	
$E^0$	Standard electrode potential	0	V
$\Delta E$	Temperature coefficient	0	V/K
<i>ORR</i> <sup>21,25</sup>			
$i_{00}$	Exchange current density at reference conditions (80°C, 101.3 kPa H <sub>2</sub> )	$2.47 \cdot 10^{-8}$	A/cm <sup>2</sup> <sub>Pt</sub>
$E^{\text{act}}$	Activation energy	67	kJ/mol
$\gamma$ (O <sub>2</sub> )	Oxygen reaction order	0.79	
$\alpha_C$	Cathodic transfer coefficient	1	
$E^0$	Standard electrode potential	1.2291	V
$\Delta E$	Temperature coefficient	$-8.456 \cdot 10^{-4}$	V/K
<i>OER</i> <sup>21</sup>			
$i_{00}$	Exchange current density at reference conditions (80°C, 101.3 kPa H <sub>2</sub> )	$1.89 \cdot 10^{-9}$	A/cm <sup>2</sup> <sub>Pt</sub>
$E^{\text{act}}$	Activation energy	38	kJ/mol
$\gamma$ (H <sub>2</sub> O)	Water reaction order	0.88	
$\alpha_A$	Anodic transfer coefficient	0.65	
$E^0$	Standard electrode potential	1.2291	V
$\Delta E$	Temperature coefficient	$-8.456 \cdot 10^{-4}$	V/K
<i>COR</i>			
$i_{00}$	Exchange current density	<i>conventional / graphitized</i> (11, 12, 21)	
$E^{\text{act}}$	Activation energy	$1.03 \cdot 10^{-18} / 2.17 \cdot 10^{-19}$	
$\alpha_C$	Cathodic transfer coefficient	134 / 140	
$E^0$	Standard electrode potential	0.67 / 0.65	
$\Delta E$	Temperature coefficient	0.2073	
		$-8.53 \cdot 10^{-4}$	
$i_{\text{H}_2\text{-cross}}^*$	Thickness normalized reference H <sub>2</sub> crossover (80°C, 101.3 kPa H <sub>2</sub> )	$5.2 \cdot 10^{-6}$	A · cm/cm <sup>2</sup>
$E^{\text{act}}$	Effective activation energy	27	kJ/mol

polarization curves and is marked by the four vertical lines in Figure 3. It is obvious that these intersects occur at higher values of  $I_{\text{SUSD}}/A_{\text{cell}}$  in the case of MEAs based on conventional carbon supports (solid lines) compared to MEAs with graphitized carbon supports (dashed lines). Furthermore, Figure 3 also predicts a rather large decrease of  $I_{\text{SUSD}}/A_{\text{cell}}$  when lowering the temperature from 80 to 5°C (red vs. blue lines), by a factor of  $\approx 8$  for conventional C MEAs and  $\approx 5$  for graphitized C MEAs.

In order to quantify the quasi-steady-state COR current density in the electrolytic part of the cell, the determined  $I_{\text{SUSD}}/A_{\text{cell}}$  values must be multiplied by the fractional contribution from the COR ( $\chi_{\text{COR}}$ ), i.e., by the fraction of  $i_{\text{EL}}$  provided by the COR:

$$\chi_{\text{COR}} = \frac{i_{\text{COR}}^{\text{cathode}}}{i_{\text{COR}}^{\text{cathode}} + i_{\text{OER}}^{\text{cathode}}} \quad [19]$$

For conventional carbon supports,  $\chi_{\text{COR}}$  is essentially one at 80°C (solid red square in Figure 3) and  $\chi_{\text{COR}} \approx 0.85$  at 5°C (solid blue square in Figure 3), which is due to the fact that the COR kinetics are much faster than the OER kinetics for Pt catalysts with conventional carbon supports. On the other hand, for graphitized carbon supports,  $\chi_{\text{COR}} \approx 0.75$  at 80°C (open red circle in Figure 3) and drops to  $\chi_{\text{COR}} \approx 0.1$  at 5°C (open blue circle in Figure 3), reflecting both the more similar COR and OER kinetics for Pt catalysts with graphitized carbon supports and the much higher activation energy for the COR compared to the OER (see Table II).

The thus obtained value of  $\chi_{\text{COR}} \cdot I_{\text{SUSD}}/A_{\text{cell}}$  represents the COR current which flows in the electrolysis part of the cell for a H<sub>2</sub>/air<sub>anode</sub> front position of  $\tau = 0.5$  (i.e., located towards the *anode* outlet during start-up and towards the *anode* inlet during shut-down) referenced to the *entire* active area of the cell ( $A_{\text{cell}}$ ). In the case where capacitive effects are negligible (i.e., for residence times between 1.3 and 2.4 s as applied in this study, as discussed above),  $I_{\text{SUSD}}$  and  $\chi_{\text{COR}}$  are identical for the start-up and the shut-down process, so that  $\chi_{\text{COR}} \cdot I_{\text{SUSD}}/A_{\text{cell}}$  is indeed a reasonably good measure for the effective average carbon oxidation current density at *each location* of the *cathode* active area over a complete SUSD cycle. This was shown in SUSD experiments, where the distribution of the carbon oxidation rate was measured either by local CO<sub>2</sub> evolution measurements,<sup>17</sup> or where it was inferred from local cathode thinning measurements,<sup>22</sup> both showing that the local carbon support oxidation over a complete SUSD cycle is reasonably constant, with slightly more damage occurring in the mid-point position.<sup>17,22</sup> This is the reason why the analysis shown in Figure 3, at a fixed H<sub>2</sub>/air<sub>anode</sub> front position of  $\tau = 0.5$ , has been used previously to estimate the area averaged SUSD damage.<sup>22</sup>

As a matter of fact, Gu et al.<sup>22</sup> stated that the carbon oxidation currents obtained in an analysis with  $\tau = 0.5$  (as done in Figure 3) are representative not only of the area averaged but also of the residence time averaged damage. That this is indeed the case can be seen from Figure 4, where  $\chi_{\text{COR}} \cdot I_{\text{SUSD}}/A_{\text{cell}}$  and  $\chi_{\text{COR}}$  are shown vs. the H<sub>2</sub>/air<sub>anode</sub> front position ( $\tau$ ) for both conventional and graphitized cathode carbon supports. Clearly, as one would expect, the magnitude of the predicted average COR current density strongly depends on the

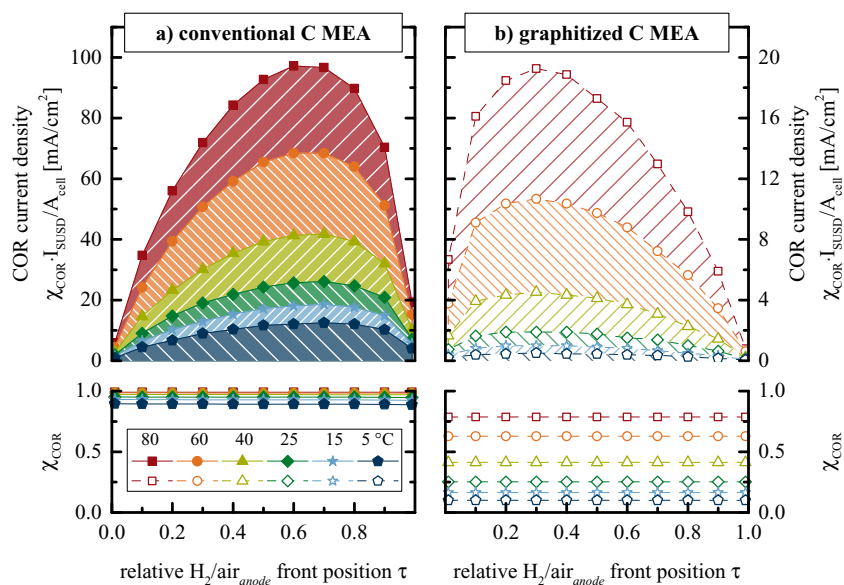


**Figure 4.** Upper panel: Carbon oxidation reaction (COR) current densities averaged over the *cathode* active area for SUSD temperatures from 5 - 80°C (see legend in lower left panel) versus relative H<sub>2</sub>/air<sub>anode</sub> front position ( $\tau = 0$  means only air is in the *anode*,  $\tau = 1$  means only H<sub>2</sub> is in the *anode*) on a) conventional and b) graphitized cathode carbon supports. Lower panel: fractions of the SUSD current consumed by the COR ( $\chi_{COR}$ ; see Equation 19) for each carbon support type. Note that the COR current density scale is different by a factor of 5 for a) and b).

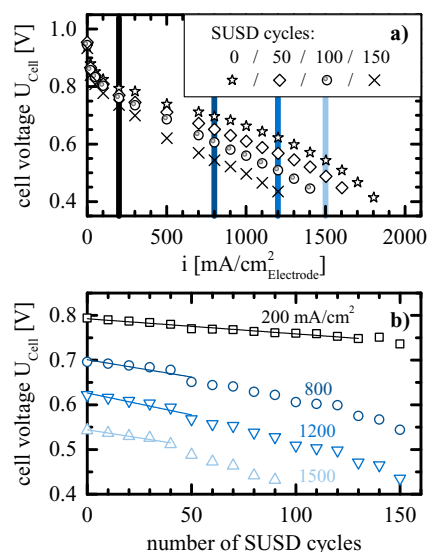
H<sub>2</sub>/air<sub>anode</sub> front position, with a maximum value near  $\tau \approx 0.6$  for conventional carbon supports (upper panel of Figure 4a) and near  $\tau \approx 0.3$  for graphitized carbon supports (upper panel of Figure 4b), whereby the predicted COR currents are clearly higher on conventional than on graphitized carbon supports. Interestingly, the extent of the SUSD current going into the COR vs. the OER is essentially independent of the H<sub>2</sub>/air<sub>anode</sub> front position (see lower panels in Figure 4). The SUSD damage averaged over the passage of the H<sub>2</sub>/air<sub>anode</sub> front (i.e., averaged over the H<sub>2</sub>/air<sub>anode</sub> front residence time) then corresponds to the COR current density integrated over the front position  $\tau$ , indicated by the hatched areas below each curve in Figures 4a and 4b.

Table III shows the different COR current densities estimated from either the approximate analysis at a fixed  $\tau$  value of 0.5 or from a more precise integration over  $\tau$ . While the latter yields  $\approx 30\%$  lower values, this difference is independent of both temperature and carbon type, so that the more simple analysis at a fixed value of  $\tau = 0.5$  should be able to capture the temperature and materials dependence of the SUSD damage. Nevertheless, for the remainder of this study, we used the values obtained by integration over  $\tau$ , in order to avoid any potential ambiguities.

## Results and Discussion

Figure 5a shows a typical set of polarization curves for a graphitized C MEA after 0, 50, 100 and 150 H<sub>2</sub>/air<sub>anode</sub> front start-up/shut-

down cycles on the *anode* side (SUSD cycles) while air is continuously flowing through the *cathode*. By comparing the initial polarization curve with the set of polarization curves after SUSD cycling (shown after 50, 100, and 150 cycles), the observed voltage losses are obviously more severe at higher current densities than in the low current density region. This is commonly explained with the oxidation of the *cathode* catalyst carbon support, and the subsequently increased mass transport resistance due to structural changes and, ultimately, the collapse of the porous electrode structure. On the other hand, the voltage losses observed at low current densities are mainly attributed to the



**Figure 5.** a) Representative H<sub>2</sub>/air polarization curves before and after 50, 100, and 150 SUSD cycles (1 cycle = 1 shut-down + 1 start-up) with a H<sub>2</sub>/air<sub>anode</sub> front residence time of  $\approx 1.3$  s; b) corresponding cell voltages U<sub>cell</sub> as function of performed SUSD cycles for four selected current densities ( $\square/\circ/\nabla/\Delta$  symbols for 200/800/1200/1500 mA/cm<sup>2</sup>, marked by vertical lines in a), with linear trend lines up to 50 mV voltage loss, from which the SUSD degradation rates are obtained. H<sub>2</sub>/air polarization curve conditions: T<sub>cell</sub> = 80°C, RH = 0.66, p<sub>cell</sub> = 70 kPa<sub>gauge,inlet</sub>, s = 1.5H<sub>2</sub>/1.8air; SUSD conditions: T<sub>cell</sub> = 80°C, RH = 1.0, p<sub>cell</sub> = 50 kPa<sub>gauge,inlet</sub>, H<sub>2</sub> and air<sub>anode</sub> flow rates at the *anode* as well as cathode air flow rates were all kept at 113 nccm, 50 cm<sup>2</sup> MEA with graphitized carbon supported electrodes, 0.1/0.4 mg<sub>pt</sub>/cm<sup>2</sup> Electrode (*anode/cathode*), 15  $\mu$ m low-EW PFSA membrane.

**Table III.** Comparison of COR current densities calculated either from assuming a fixed value of  $\tau = 0.5$  (i.e., when the H<sub>2</sub>/air<sub>anode</sub> front has passed half of the cell) or from properly integrating over the range of  $0.01 \leq \tau \leq 0.99$ . Calculations were done for conventional cathode carbon supports (“Conventional C MEA”) and graphitized cathode carbon supports (“Graphitized C MEA”), for temperatures between 5 and 80°C and for RH = 1 and a cell pressure of 50 kPa<sub>gauge</sub>. The lowest line for each carbon type is the ratio of the values obtained by the two different methods.

	COR current density [mA/cm <sup>2</sup> ]	T [°C]	relative H <sub>2</sub> /air <sub>anode</sub> front position $\tau$					
			80	60	40	25	15	5
Conventional C MEA	integrated		70	50	30	19	13	9.1
	$\tau = 0.5$		93	65	39	24	17	12
	ratio		1.3	1.3	1.3	1.3	1.3	1.3
Graphitized C MEA	integrated		14	7.7	3.3	1.4	0.7	0.4
	$\tau = 0.5$		17	9.7	4.1	1.8	0.9	0.5
	ratio		1.3	1.3	1.3	1.3	1.3	1.3

decrease of the electrochemically active surface area (ECSA).<sup>11</sup> In order to quantify the voltage losses in both the high and low current density region, cell voltages as a function of conducted SUSD cycles at four different current densities are plotted in Figure 5b. Here, linear trend lines up to an SUSD induced voltage loss of 50 mV were fitted (least-square regression), from which the linearized SUSD degradation rate used throughout this work was determined (in units of mV/cycle). It should be noted that the thus determined degradation rates do depend on the selected voltage loss range, owing to the increasing non-linearity of the voltage loss vs. the number of SUSD cycles with increasing voltage loss. In our study we observed a reasonably linear behavior up to voltage losses of 50 mV, which may be compared to other cut off values used in the literature (e.g., 30 mV in Reference 27 or 100 mV in Reference 12). The value of 50 mV chosen here is, we believe, a good compromise between obtaining a sufficiently linear response and the maximum acceptable SUSD loss in automotive applications, especially considering that SUSD induced voltage losses are only one of the various contributions to cell voltage degradation during fuel cell lifetime.<sup>27</sup>

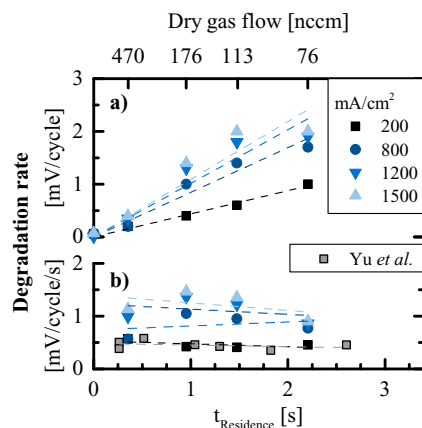
**Residence time normalized SUSD degradation rates.**—The  $H_2/air_{anode}$  front residence time for accelerated SUSD degradation tests is usually on the order of  $\approx 1$  s. However, practically relevant residence times in fuel cell applications are more like on the order of  $\approx 0.1$  s.<sup>15</sup> Thus, to project SUSD-induced degradation rates from accelerated SUSD tests towards automotive timescales, a more general definition of the degradation rate – independent of the actual  $H_2/air_{anode}$  front residence time  $t_{Residence}$  – is desirable. Yu et al. demonstrated for low polarization current densities, that the degradation rate is linearly correlated with  $t_{Residence}$ ,<sup>12</sup> allowing for a normalization of the degradation rate to  $t_{Residence}$ . It should be noted that for very short residence times ( $< 0.5$  s<sup>13</sup>), capacitive effects may lead to lower  $t_{Residence}$  normalized SUSD degradation rates than those determined from accelerated tests,<sup>22</sup> but the latter nevertheless provide a reasonably good estimate. The residence time is calculated from the applied dry gas flow rate under standard conditions ( $\dot{V}_0^{dry}$  in units of nccm), the internal flow-field volume ( $V^{FF} = 2.35$  cm<sup>3</sup>), and the void volume of the compressed gas diffusion layer ( $V^{GDL} \approx 0.72$  cm<sup>3</sup>), whereby the actual wet gas flow rate ( $\dot{V}_{T,p,RH}^{wet}$ ) at any given temperature (T), RH, and cell pressure ( $p_{cell}$ ) is calculated from the water saturation pressure ( $p_T^{H_2O,sat.}$ ) and the ideal gas law:

$$t_{Residence} = \frac{V^{FF} + V^{GDL}}{\dot{V}_{T,p,RH}^{wet}} = \frac{V^{FF} + V^{GDL}}{\dot{V}_0^{dry} \cdot \frac{p_0}{p_{gas}} \cdot \frac{T}{T_0}} \quad [20]$$

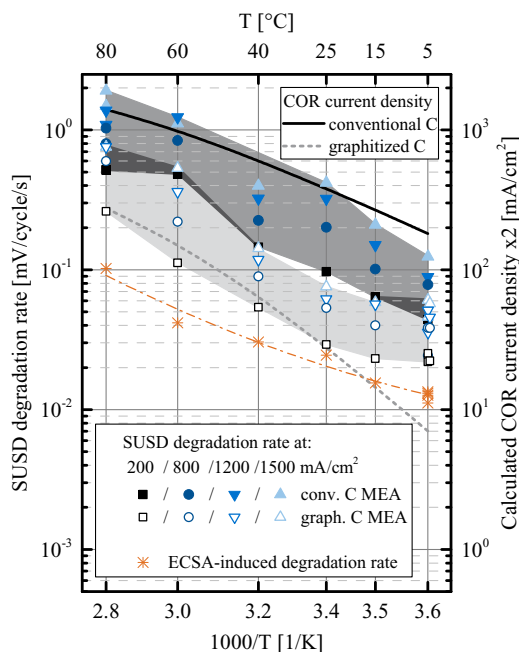
Here,  $T_0 = 273.15$  K,  $p_0 = 101.3$  kPa, and  $p_{gas} = p_{cell} - p_{H_2O} = p_{cell} - RH \cdot p_T^{H_2O,sat.}$

Figure 6a shows the degradation rates (linearized for up to 50 mV voltage loss and in units of mV/cycle) for various current densities as a function of  $t_{Residence}$ , measured for conventional C MEAs at 80°C. Apparently, the correlation between degradation rate and  $t_{Residence}$  is rather linear, starting to deviate only at residence times approaching  $\approx 2$  s. This can possibly be attributed to *i*) diffusional broadening of the  $H_2/air_{anode}$  front at low gas flow rates in the experimental set-up and/or *ii*) to reactant depletion in the flow-field at long residence times, as reported by Yu et al.<sup>13</sup> Figure 6b re-plots the data normalized to  $t_{Residence}$  (i.e., in units of mV/cycle/s), including data reported by Yu et al.,<sup>12</sup> at 200 mA/cm<sup>2</sup> which are in excellent agreement with our measurements. Furthermore, the  $t_{Residence}$  normalized degradation rates for each current density are reasonably independent of residence time, rendering the normalization of SUSD degradation rates to the  $H_2/air_{anode}$  front residence time a good approximation over the investigated residence time range.

**Measured vs. projected temperature dependent SUSD degradation rates.**—Figure 7 summarizes the residence time normalized SUSD degradation rates (in mV/cycle/s) versus temperature in an Arrhenius type plot at various current densities for conventional C MEAs



**Figure 6.** SUSD degradation rates for conventional C MEAs at various current densities (1 cycle  $\equiv$  1 shut-down + 1 start-up) vs.  $H_2/air_{anode}$  front residence time (determined by Equation 20 for the dry gas flow rates shown in the upper y-axis, in terms of: a) voltage loss per SUSD cycle; b) residence time ( $t_{Residence}$ ) normalized degradation rates. Linear trend lines are indicated by dashed lines, and the values reported by Yu et al.<sup>12</sup> for 200 mA/cm<sup>2</sup> are given for comparison (grey squares).  $H_2/air$  polarization curve conditions:  $T_{cell} = 80^\circ\text{C}$ ,  $RH = 0.66$ ,  $p_{cell} = 70$  kPa<sub>gauge,inlet</sub>,  $s = 1.5H_2/1.8air$ ; SUSD conditions:  $T_{cell} = 80^\circ\text{C}$ ,  $RH = 0.66$ ,  $p_{cell} = 50$  kPa<sub>gauge,inlet</sub>,  $H_2$  and  $air_{anode}$  flow rates at the anode as well as cathode air flow rates were all kept at 113 nccm. 50 cm<sup>2</sup> MEA (Gore Primea Mesga) with 0.1/0.4 mgPt/cm<sup>2</sup> Electrode (anode/cathode) and an 18  $\mu\text{m}$  reinforced PFSA membrane.



**Figure 7.** Arrhenius-type plot on the temperature dependence of the  $t_{Residence}$  normalized SUSD degradation rates (plotted on left y-axis) at different current densities for conventional C MEAs (solid symbols) and for graphitized C MEAs (open symbols). Also shown on the right y-axis are the SUSD induced carbon corrosion current densities predicted by our model for conventional C MEAs (solid line) and for graphitized C MEAs (dashed line), which are also listed in Table III (“integrated” values). The orange asterisks show the  $t_{Residence}$  normalized degradation rates caused by the experimentally determined ECSA loss on graphitized C MEAs (cf. Table IV); the orange dash-dotted line is a guide-to-the-eye).  $H_2/air$  polarization curve conditions:  $T_{cell} = 80^\circ\text{C}$ ,  $RH = 0.66$ ,  $p_{cell} = 70$  kPa<sub>gauge,inlet</sub>,  $s = 1.5H_2/1.8air$ ; SUSD conditions: variable  $T_{cell}$ ,  $RH \approx 1.0$ ,  $p_{cell} = 50$  kPa<sub>gauge,inlet</sub>,  $H_2$  and  $air_{anode}$  flow rates at the anode as well as cathode air flow rates were all kept at 113 nccm, corresponding to  $H_2/air_{anode}$  front residence times of  $\approx 1.3 - 2.4$  s for 80/5°C (see Equation 20). Repeat experiments can be identified by multiple symbols at the same temperature.

(solid symbols) and graphitized carbon MEAs (open symbols). At 80°C, the experimentally determined 2 - 3 times lower SUSD degradation rates for graphitized C MEAs are in good agreement with the factor of 2.5 - 3.5 determined at 0.2 - 1.2 A/cm<sup>2</sup> by Yu et al.<sup>13</sup> To the best of our knowledge, Figure 7 is the first systematic study of the temperature dependence of SUSD degradation rates, quantifying the decrease of the SUSD degradation rates from 80 to 5°C, by a factor of  $\approx 10 - 15$  for conventional cathode carbon supports (upper shaded area in Figure 7) and by a similar factor of  $\approx 10 - 15$  for graphitized cathode carbon supports (lower shaded area in Figure 7). It is interesting to note, however, that the SUSD degradation rate decreases faster with temperature for graphitized C MEAs in between 80°C and room temperature, but that their SUSD degradation rate at low temperatures exhibits a substantially weaker temperature dependence. As a consequence, below room temperature, the SUSD degradation rates of graphitized and conventional C MEAs are approaching each other, so that the SUSD stability advantage of graphitized carbon supports over conventional carbon supports apparently diminishes. This raises the question whether graphitized carbon supports will offer significant advantages over conventional carbon supports with regards to SUSD degradation, since SUSD effects in state-of-the-art fuel cell systems mostly occur at low temperatures (see Introduction).

Next we will compare the temperature and carbon support dependence of the measured  $t_{\text{Residence}}$  normalized SUSD degradation rates with our modeled COR oxidation rates. In the range where the voltage loss vs. the number of conducted SUSD cycles is roughly linear and under the assumption that the slight variation of carbon oxidation across the cathode active area can be neglected, it is reasonable to assume that the modeled COR oxidation rates (see “integrated” values in Table III) be roughly proportional to the  $t_{\text{Residence}}$  normalized SUSD degradation rates. The calculated COR current densities are plotted on the right y-axis in Figure 7 for both conventional C MEAs (solid line) and graphitized C MEAs. The difference in COR current density for conventional and graphitized MEAs at 80°C is a factor of  $\approx 5$  (see solid vs. dashed line in Figure 7) and thus larger than the experimentally observed difference in SUSD degradation rates of  $\approx 3$  (see solid vs. open symbols in Figure 7). Nevertheless, considering all the simplifying assumptions and the limited accuracy of the kinetic parameters (particularly for the COR) required for the model (see Table II), a prediction within a factor of  $\approx 2$  is quite good.

A further, implicit simplification of our model is that the COR oxidation rates are calculated based on beginning-of-life (BOL) polarization curves, neglecting that the gradually degrading cathode electrode is increasingly hindering the ORR on the FC part of the cell at increasing numbers of SUSD events (see Figure 1). This would, in principle lead to lower internal SUSD currents  $I_{\text{SUSD}}$ , thus finally lowering COR oxidation rates (see Equations 11 and 12) over the course of SUSD cycling experiments. One can try to give a rule-of-thumb estimate for the magnitude of this effect. Local ORR current densities occurring during SUSD can be obtained from Figure 4, dividing the y-axis by  $\chi_{\text{COR}}$  and by  $\tau$  (cf. Equation 11; H<sub>2</sub> crossover is negligible at the relevant current densities). As a result, the highest local current densities are on the order of 0.2 - 0.3 A/cm<sup>2</sup> (in the worst case, i.e., for conventional C MEAs at 80°C). From the diagnostic polarization curves taken in between SUSD cycles, the EOL (end-of-life) polarization loss (defined to be 50 mV compared to the BOL value) at 200 mA/cm<sup>2</sup> is known (although the polarization curves in the study were not performed at identical conditions as the SUSD experiments, we take this value as an estimate for the penalty due to hindered oxygen mass transport during SUSD at EOL). However, comparing the calculated COR current density not only to the experimental degradation rates obtained at 200 mA/cm<sup>2</sup>, but also to those obtained at 800, 1200 and 1500 mA/cm<sup>2</sup> where the EOL criterion of 50 mV loss is fulfilled after different numbers of SUSD cycles for each current density, a representative average needs to be found in order to reference it to the calculated COR current density. A reasonable means could be one of the intermediate current densities (800 or 1200 mA/cm<sup>2</sup>), where approximately half the number of cycles necessary to reach

50 mV performance loss compared to 200 mA/cm<sup>2</sup> (an analogue plot to Figure 5 but for conventional C MEAs would show this). This means, that at 200 mA/cm<sup>2</sup>, which we use as a prediction for the hindrance of  $I_{\text{SUSD}}$  over the number of cycles performed, we can expect  $\approx 0.5 \cdot 50 \text{ mV} = 25 \text{ mV}$  mass transport penalty. If one translates this into a projected difference of  $I_{\text{SUSD}}$  (see Equation 3), it would mean a reduction to  $\approx 45\%$  of the initial value at EOL, and (assuming linear behavior over SUSD cycles) to  $\approx 73\%$  on average. Note that exercising this estimation for lower temperatures and for graphitized C MEAs yields significantly lower BOL values for  $I_{\text{SUSD}}$ , thus lower local oxygen reduction current densities during SUSD, ultimately leading to less significant decay of COR current density over the SUSD cycling experiments. In conclusion, the error introduced by ignoring the decay in polarization curves over SUSD cycles on the COR current density would be largest for conventional C MEAs at high temperatures, while this error is minor for graphitized C MEAs over the full temperature range and for conventional C MEAs at low temperatures. Thus, the left hand side of the full line in Figure 7 would be shifted slightly to lower values (to  $\approx 73\%$  of its shown value), while shifting the right hand side (low temperatures) as well as the complete dashed line (projected COR current densities on graphitized C MEAs) only marginally. Admittedly, this would qualitatively lower the factor for the projected COR currents of conventional C MEAs between 5 and 80°C. However, as this rough estimate has to rely on many additional assumptions – appropriate cycle number, cell voltage penalty (only estimated from polarization curves, etc.) – with associated uncertainties and as the resulting change of  $< 30\%$  is presumably small compared to the overall precision of the model, it is not being considered in the further analysis.

In the case of conventional C MEAs, temperature dependence of the projected (solid line) and experimentally determined  $t_{\text{Residence}}$  normalized SUSD degradation rates (solid symbols) are in good agreement, with a projected factor of  $\approx 8$  versus an experimentally observed factor of  $\approx 10 - 15$  between 5 and 80°C (see Figure 7). On the other hand, for graphitized C MEAs, the projected (dashed line) and measured (open symbols) temperature dependence only agrees for temperatures between 25 and 80°C (projected factor of  $\approx 10$  vs. measured factor of  $\approx 10 - 15$ ), while at  $T < 25^\circ\text{C}$ , the measured degradation rates display a much weaker temperature dependence than what would be predicted by the model. Quite obviously, the in comparison to conventional C MEAs projected increasingly superior SUSD stability of graphitized C MEAs with decreasing temperature (see Table III and solid vs. dashed lines in Figure 3) is at variance with our experimental SUSD data. As the model solely takes into account carbon corrosion to project performance loss, this suggests that some other degradation mechanism may become governing under conditions where the SUSD induced carbon corrosion becomes very small (i.e., at low temperatures and for graphitized supports).

With experimental  $t_{\text{Residence}}$  normalized degradation rates in the vicinity of 0.03 mV/cycle/s, it may be hypothesized that the predominant degradation mechanism transitions from structural electrode degradation induced by carbon oxidation to voltage losses caused by a loss of the electrochemically active surface area ( $A_{\text{Pt}}$ ). This would be consistent with the high activation energy for the COR (see Table II) and the fact that a large number of SUSD cycles is required at low temperatures to result in a voltage loss of 50 mV for which we determined the linearized SUSD degradation rates. To test this hypothesis, one can examine the change of the electrochemically active surface area of the cathode of the graphitized C MEA over the number of SUSD cycles. Figure 8 shows the electrochemically active surface area obtained by cyclic voltammetry and normalized to its BOL value ( $[A_{\text{Pt}}]_{\text{cycle\#}}/[A_{\text{Pt}}]_{\text{BOL}}$ ), with  $[A_{\text{Pt}}]_{\text{BOL}} = 42 \text{ m}^2/\text{g}_{\text{Pt}}$  (see Table I) vs. the number of SUSD cycles. From Figure 8 one can now determine the remaining platinum surface area at the number of SUSD cycles at which the SUSD degradation rate was determined, i.e., the number of SUSD cycles where the voltage loss at 0.2 A/cm<sup>2</sup> amounted to 50 mV, furtheron referred to as end-of-life condition (EOL). These are indicated by the dashed vertical lines in Figure 8 (see also 4<sup>th</sup> column in Table IV), together with the remaining normalized Pt surface

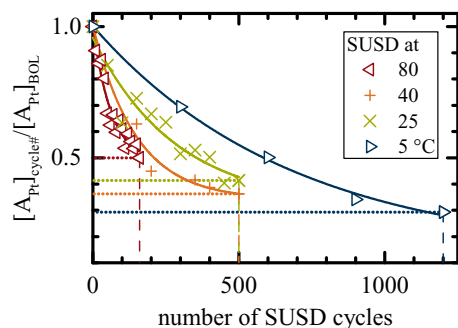


**Figure 8.** Relative remaining electrochemically active platinum surface area of *cathode* electrode ( $[A_{Pt}]_{cycle\#}/[A_{Pt}]_{BOL}$ ) as a function of the number of SUSD cycles conducted on graphitized C MEAs. The number of SUSD cycles at which a 50 mV SUSD loss at 0.2 A/cm<sup>2</sup> was obtained is indicated by vertical dashed lines, together with the relative platinum surface area at this point (referred to as end-of-life (EOL)). The testing protocol for these data is the same as that listed in the caption of Figure 7.

area ( $[A_{Pt}]_{EOL}/[A_{Pt}]_{BOL}$ ; s. dotted horizontal lines in Figure 8 and 2<sup>nd</sup> column in Table IV).

From  $[A_{Pt}]_{EOL}/[A_{Pt}]_{BOL}$  one can estimate the ORR kinetic loss caused by the loss of active platinum surface area, which can be derived from Equation 3:

$$\Delta E_{ORR}^{cathode} = \frac{RT}{\alpha_c F} \cdot \ln([A_{Pt}]_{EOL}/[A_{Pt}]_{BOL}) \quad [21]$$

where  $\alpha_c = 1$  (see Table II). The *apparent*  $t_{Residence}$  normalized SUSD degradation rate due to the purely ORR kinetic losses, calculated from the measured Pt surface area loss, is then simply described by  $\Delta E_{ORR}^{cathode}/(\#SUSD_{EOL} \cdot t_{Residence})$ . This analysis is summarized in Table IV for the SUSD experiments on the graphitized C MEAs between 5 and 80 °C. The *apparent*  $t_{Residence}$  normalized SUSD degradation due to the loss of Pt surface area is also shown in Figure 7, (orange asterisks), illustrating that the purely kinetic ORR voltage losses due to Pt surface area loss with graphitized C MEAs are significantly below the overall SUSD degradation rates at high temperatures, but represent a more and more significant fraction at room temperature and below. This is also reflected by the temperature dependence of the SUSD degradation rate of graphitized C MEAs, which follows the trend predicted by the kinetic carbon oxidation model at high temperatures, while it follows the trend predicted by the Pt surface area loss induced ORR kinetic voltage loss at room temperature and below.

**Table IV.** Relative loss of active platinum surface area ( $[A_{Pt}]_{EOL}/[A_{Pt}]_{BOL}$ ) from beginning-of-life (BOL) to end-of-life (EOL), whereby the latter is defined at a H<sub>2</sub>/air performance loss of 50 mV at at 0.2 A/cm<sup>2</sup> and the number of SUSD cycles up to this point are referred to as  $\#SUSD_{EOL}$ . These values are obtained from the data shown in Figure 8 for the different SUSD temperatures ( $T_{SUSD}$ ). The ORR kinetic loss ( $\Delta E_{ORR}^{cathode}$ ) caused by the relative Pt surface area loss is calculated by Equation 21. The *apparent* degradation rate predicted purely by the platinum surface area loss (last column) corresponds to  $\Delta E_{ORR}^{cathode}/(\#SUSD_{EOL} \cdot t_{Residence})$ .

$T_{SUSD}$ °C	$[A_{Pt}]_{EOL}/$ $[A_{Pt}]_{BOL}$	$\Delta E_{ORR}^{cathode}$ mV	$\#SUSD_{EOL}$ SUSD cycles	$t_{Residence}$ s	app. deg. rate mV/cycle/s
5	0.29	37	1200	2.4	0.013
5	0.45	24	800	2.4	0.013
5	0.46	24	900	2.4	0.011
5	0.38	29	900	2.4	0.013
15	0.52	20	560	2.3	0.016
25	0.41	27	500	2.2	0.025
40	0.36	31	500	2.0	0.030
60	0.53	20	270	1.7	0.042
80	0.50	21	160	1.3	0.102

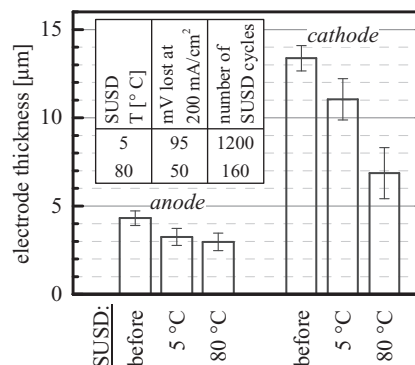


**Figure 9.** *Anode* and *cathode* electrode thicknesses of graphitized C MEAs before and after SUSD cycling at 5 and 80 °C determined by scanning electron microscopy cross-sections (see Experimental section). The inset shows the total number of SUSD cycles each MEA underwent until cross-sectional imaging was done and the associated voltage loss during a polarization curve at 200 mA/cm<sup>2</sup> with respect to the initial performance.

The hypothesis that the SUSD degradation rate on the graphitized C MEA transitions from a predominantly carbon corrosion induced to a Pt surface area loss induced mechanism as the SUSD temperature is decreased from 80 °C to 5 °C, is further supported by the observed electrode thinning dependence on SUSD temperature (Figure 9). Apparently, at 80 °C the EOL *cathode* thickness is only  $\approx 50\%$  its initial value (at 50 mV performance loss at 0.2 A/cm<sup>2</sup>; see inset in Figure 9), indicating a structural collapse of the electrode which requires a carbon weight loss  $\geq 10$  wt%.<sup>12,24</sup> On the other hand, at 5 °C the remaining thickness is  $> 80\%$  of its initial value (after a much higher performance loss of 95 mV at 0.2 A/cm<sup>2</sup>; see inset in Figure 9), indicating that the electrode structure remains essentially intact and that the carbon weight loss must be  $\ll 10$  wt%.<sup>12,24</sup>

At last, one may consider the question whether the effective 0  $\leftrightarrow$  1 V potential cycling of the *anode* produced by the H<sub>2</sub>/air<sub>anode</sub> front might lead to carbon corrosion of at the anode, which is known to occur also upon potential cycling between 0 V (H<sub>2</sub> part of the H<sub>2</sub>/air<sub>anode</sub> front) and 1 V vs. reversible hydrogen electrode (air part of the H<sub>2</sub>/air<sub>anode</sub> front),<sup>28,29</sup> with substantial carbon corrosion rates even measured for cycles between 0.4 and 0.95 V.<sup>30</sup> Measurements of the anode thickness indeed show that it decreases by  $\approx 25\%$  over the course of extended SUSD cycles (Figure 9), but this seems to be independent of whether the SUSD tests were conducted at 5 °C or at 80 °C. Therefore, we believe that the temperature dependence of the SUSD degradation is not related to voltage cycling induced degradation of the anode.

In conclusion, the degradation rate due to SUSD cycles is mitigated by both changing carbon support from conventional to graphitized carbon and by decreasing the SUSD temperature. While for the tested graphitized C MEAs a temperature decrease below 25 °C did not lower the SUSD degradation rate anymore, this can well be explained by the loss of electrochemically active surface area (i.e., by the effect of Pt surface area loss on the ORR kinetics) rather than by carbon corrosion becoming limiting at low temperatures.

## Conclusions

In this study, we present the first systematic data set of degradation rates induced by repeated SUSD cycling between 5 and 80 °C for both MEAs with conventional carbon supports and graphitized carbon supports in the catalyst layers. In both cases, the degradation rates obtained via polarization curves and expressed as H<sub>2</sub>/air<sub>anode</sub> front time normalized voltage loss per cycle SUSD decrease by a factor of  $\approx 10$  from 80 to 5 °C. For conventional C MEAs, this trend is in good accordance with carbon corrosion currents projected over the same temperature range by a kinetic model, slightly modified from the one presented by Gu et al.<sup>22</sup> For graphitized C MEAs, in

contrast, the kinetic model predicts a much stronger effect of temperature (factor of  $\approx 39$  between 5 and 80°C). This discrepancy can be explained by the significant contribution from voltage cycling induced platinum surface area loss and the associated ORR kinetic loss. The latter exhibits a much weaker dependency on temperature than the carbon corrosion currents projected by the kinetic model. Thus, at elevated SUSD temperatures (80 – 25°C) performance degradation is limited by carbon corrosion, whereas the kinetic penalty due to platinum surface area loss is determining performance losses below 25°C, resulting in levelling-off overall degradation rate in this temperature range. For this reason, at SUSD temperatures relevant for state-of-the-art PEMFC systems (near/below room temperature), the apparent SUSD degradation rates on graphitized carbon supports are only better by a factor of 2 compared to conventional carbon supports.

### Acknowledgments

Financial support by Volkswagen AG and the supply of graphitized carbon electrodes by Greenerity GmbH are gratefully acknowledged. We would like to thank Patrick Zihrl from the fuel cell research department of Volkswagen AG for fruitful discussions and for reviewing the manuscript. We would also like to thank Balsu Lakshmanan from General Motors for pointing out the origin of the change in the aging mechanism at low SUSD temperatures. Philipp Rheinländer is acknowledged for the installation of the MEA cross section process line at TEC.

### References

1. Hyundai Motor Co. Global PR (accessed 08/23/2016), <http://globalpr.hyundai.com/prCenter/news/newsView.do?dID=2989>.
2. Toyota Motor Co. News Releases 2014 (accessed 05/20/2016), <http://newsroom.toyota.co.jp/en/detail/4198334/>.
3. Honda Motor Co. News Releases 2016 (accessed 05/20/2016), <http://world.honda.com/news/2016/4160310eng.html>.
4. J. C. Mankins, *Technology Readiness Levels: A White Paper* (1995, accessed 05/20/2016), <http://www.hq.nasa.gov/office/codeq/trl/trl.pdf>.
5. R. Borup, J. Meyers, B. Pivovar, Y. S. Kim, R. Mukundan, N. Garland, D. Myers, M. Wilson, F. Garzon, D. Wood, P. Zelenay, K. More, K. Stroh, T. Zawodzinski, J. Boncella, J. E. McGrath, M. Inaba, K. Miyatake, M. Hori, K. Ota, Z. Ogumi, S. Miyata, A. Nishikata, Z. Siroma, Y. Uchimoto, K. Yasuda, K.-i. Kimijima, and N. Iwashita, *Chem. Rev.*, **107**, 3904 (2007).
6. C. A. Reiser, L. Bregoli, T. W. Patterson, J. S. Yi, J. D. Yang, M. L. Perry, and T. D. Jarvi, *Electrochem. Solid-State Lett.*, **8**, A273 (2005).
7. C. Reiser, D. Yang, and R. Sawyer, *Procedure for starting up a fuel cell system using a fuel purge*, Patent US 2002/0076582 A1.
8. P. T. Yu and F. T. Wagner, *Procedures for shutting down fuel cell system by using air purge at low cell temperature*, Patent US 7270904 B2.
9. J. E. Owejan, P. T. Yu, and R. Makharia, *ECS Trans.*, **11**, 1049 (2007).
10. H. A. Gasteiger, D. R. Baker, R. N. Carter, W. Gu, Y. Liu, F. T. Wagner, and P. T. Yu, in *Hydrogen and Fuel Cells*, D. Stolten Editor, p. 3, Wiley-VCH (2010).
11. R. N. Carter, W. Gu, B. Brady, P. T. Yu, K. Subramanian, and H. A. Gasteiger, in *Handbook of Fuel Cells - Fundamentals, Technology and Applications*, W. Vielstich, A. Lamm, and H. A. Gasteiger Editors, p. 829, John Wiley & Sons, Ltd. (2009).
12. P. T. Yu, W. Gu, R. Makharia, F. T. Wagner, and H. A. Gasteiger, *ECS Trans.*, **3**, 797 (2006).
13. P. T. Yu, W. Gu, J. Zhang, R. Makharia, F. T. Wagner, and H. A. Gasteiger, in *Polymer Electrolyte Fuel Cell Durability*, p. 29, Springer New York (2009).
14. O. Gröger, H. A. Gasteiger, and J.-P. Suchsland, *J. Electrochem. Soc.*, **162**, A2605 (2015).
15. P. T. Yu and F. T. Wagner, *Method for Shutting Down a Fuel Cell System Using an Air Purge*, Patent US 2008/0003465 A1.
16. K. H. Lim, H.-S. Oh, S.-E. Jang, Y.-J. Ko, H.-J. Kim, and H. Kim, *J. Power Sources*, **193**, 575 (2009).
17. S. Kreitmeyer, A. Wokaun, and F. N. Büchi, *J. Electrochem. Soc.*, **159**, F787 (2012).
18. Y. Y. Jo, E. Cho, J. H. Kim, T.-H. Lim, I.-H. Oh, S.-K. Kim, H.-J. Kim, and J. H. Jang, *J. Power Sources*, **196**, 9906 (2011).
19. P. Yu and F. Wagner, *Method of using H2 purge for stack startup/shutdown to improve stack durability*, Patent US 2006/0046106 A1.
20. H. Shintani, Y. Kojima, K. Kakinuma, M. Watanabe, and M. Uchida, *J. Power Sources*, **294**, 292 (2015).
21. M. L. Perry, T. Patterson, and C. Reiser, *ECS Trans.*, **3**, 783 (2006).
22. W. Gu, P. T. Yu, R. N. Carter, R. Makharia, and H. A. Gasteiger, in *Modern Aspects of Electrochemistry* vol. **49**, U. Pasaogullari and C.-Y. Wang Editors, p. 45, Springer New York (2010).
23. D. P. Davies, P. L. Adcock, M. Turpin, and S. J. Rowen, *J. Appl. Electrochem.*, **30**, 101.
24. P. T. Yu, Z. Liu, and R. Makharia, *J. Electrochem. Soc.*, **160**, F645 (2013).
25. K. C. Neyerlin, W. Gu, J. Jorne, and H. A. Gasteiger, *J. Electrochem. Soc.*, **154**, B631 (2007).
26. K. C. Neyerlin, W. Gu, J. Jorne, and H. A. Gasteiger, *J. Electrochem. Soc.*, **153**, A1955 (2006).
27. R. Makharia, S. Kocha, P. Yu, M. A. Sweikart, W. Gu, F. Wagner, and H. A. Gasteiger, *ECS Trans.*, **1**, 3 (2006).
28. L. M. Roen, C. H. Paik, and T. D. Jarvi, *Electrochem. Solid-State Lett.*, **7**, A19 (2004).
29. F. T. Wagner, S. G. Yan, and P. T. Yu, in *Handbook of Fuel Cells - Fundamentals, Technology and Applications*, W. Vielstich, H. Yokokawa, and H. A. Gasteiger Editors, p. 250, John Wiley & Sons, Ltd. (2009).
30. R. L. Borup, D. D. Papadias, R. Mukundan, D. Spornjak, D. A. Langlois, R. Ahluwalia, K. L. More, and S. Grot, *ECS Trans.*, **69**, 1029 (2015).